# Multiple motifs regulate apical sorting of p75 via a mechanism that involves dimerization and higher-order oligomerization

Robert T. Youker[a], Jennifer R. Bruns[a], Simone A. Costa[a], Youssef Rbaibi[a], Frederick Lanni[b,c], Ossama B. Kashlan[a], Haibing Teng[c], and Ora A. Weisz[a]

[a]Renal-Electrolyte Division, Department of Medicine, University of Pittsburgh School of Medicine, Pittsburgh, PA 15261; [b]Department of Biological Sciences and [c]Molecular Biosensor and Imaging Center, Carnegie Mellon University, Pittsburgh, PA 15213

**ABSTRACT** The sorting signals that direct proteins to the apical surface of polarized epithelial cells are complex and can include posttranslational modifications, such as N- and O-linked glycosylation. Efficient apical sorting of the neurotrophin receptor p75 is dependent on its O-glycosylated membrane proximal stalk, but how this domain mediates targeting is unknown. Protein oligomerization or clustering has been suggested as a common step in the segregation of all apical proteins. Like many apical proteins, p75 forms dimers, and we hypothesized that formation of higher-order clusters mediated by p75 dimerization and interactions of the stalk facilitate its apical sorting. Using fluorescence fluctuation techniques (photon-counting histogram and number and brightness analyses) to study p75 oligomerization status in vivo, we found that wild-type p75–green fluorescent protein forms clusters in the *trans*-Golgi network (TGN) but not at the plasma membrane. Disruption of either the dimerization motif or the stalk domain impaired both clustering and polarized delivery. Manipulation of *O*-glycan processing or depletion of multiple galectins expressed in Madin-Darby canine kidney cells had no effect on p75 sorting, suggesting that the stalk domain functions as a structural prop to position other determinants in the lumenal domain of p75 for oligomerization. Additionally, a p75 mutant with intact dimerization and stalk motifs but with a dominant basolateral sorting determinant (Δ250 mutant) did not form oligomers, consistent with a requirement for clustering in apical sorting. Artificially enhancing dimerization restored clustering to the Δ250 mutant but was insufficient to reroute this mutant to the apical surface. Together these studies demonstrate that clustering in the TGN is required for normal biosynthetic apical sorting of p75 but is not by itself sufficient to reroute a protein to the apical surface in the presence of a strong basolateral sorting determinant. Our studies shed new light on the hierarchy of polarized sorting signals and on the mechanisms by which newly synthesized proteins are segregated in the TGN for eventual apical delivery.

**Monitoring Editor**
Keith E. Mostov
University of California, San Francisco

Received: Feb 5, 2013
Revised: Apr 18, 2013
Accepted: Apr 19, 2013

This article was published online ahead of print in MBoC in Press (http://www.molbiolcell.org/cgi/doi/10.1091/mbc.E13-02-0078) on May 1, 2013.

Address correspondence to: Robert T. Youker (rty4@pitt.edu).

Abbreviations used: ARE, apical recycling endosome; FCS, fluorescence correlation spectroscopy; FRAP, fluorescence recovery after photobleaching; Gal, galectin; GPCR, G protein–coupled receptor; GPI, glycosylphosphatidylinositol; LEA, *Lycopersicon esculentum* agglutinin; MDCK, Madin-Darby canine kidney; N&B, number and brightness analysis; PCH, photon-counting histogram; PL, polylactosamine; ST6, ST6GalNAc-1; TGN, *trans*-Golgi network.

© 2013 Youker *et al.* This article is distributed by The American Society for Cell Biology under license from the author(s). Two months after publication it is available to the public under an Attribution–Noncommercial–Share Alike 3.0 Unported Creative Commons License (http://creativecommons.org/licenses/by-nc-sa/3.0).

"ASCB®," "The American Society for Cell Biology®," and "Molecular Biology of the Cell®" are registered trademarks of The American Society of Cell Biology.

## INTRODUCTION

The sorting of proteins to the apical or basolateral surface of polarized epithelial cells is critical for proper cell function and the maintenance of cellular architecture (for a review, see Weisz and Rodriguez-Boulan, 2009). Cell polarity is maintained in part through the selective targeting of newly synthesized proteins to their respective membrane domains (apical or basolateral). Initial segregation of cargo into distinct surface-delivery pathways occurs at the *trans*-Golgi network (TGN; Rindler *et al.*, 1984; Fuller *et al.*, 1985; Jacob and Naim, 2001; Cresawn *et al.*, 2007; Guerriero *et al.*, 2008; Folsch *et al.*, 2009). Basolateral sorting signals tend to be short amino acid motifs that reside within the cytosolic tails of cargo. In contrast, the sorting motifs for apically targeted proteins are far more complex and have been localized to lumenal, membrane, or cytosolic domains. In some cases, these sorting motifs consist of cytoplasmic or lumenal amino acid stretches within the protein, as for megalin and the P2Y2 receptor (Takeda *et al.*, 2003; Qi *et al.*, 2005). However, many apical sorting signals require posttranslational modifications, including O- or N-linked glycosylation (Lisanti and Rodriguez-Boulan, 1990; Naim *et al.*, 1999; Ihrke *et al.*, 2001; Potter *et al.*, 2006; Kinlough *et al.*, 2011) or glycosylphosphatidylinositol lipid anchors that allow preferential association with cholesterol/sphingolipid-enriched microdomains (lipid rafts; Lisanti *et al.*, 1989; Zurzolo *et al.*, 1994; Scheiffele *et al.*, 1997; Potter *et al.*, 2004, 2006; Cao *et al.*, 2012). It is unclear how these different classes of apical proteins are segregated into distinct TGN-derived transport carriers. After leaving the TGN, many apically destined proteins traffic through a second sorting station, the Rab11a-positive apical recycling endosome (ARE), en route to the surface (Cresawn *et al.*, 2007; Cramm-Behrens *et al.*, 2008; Folsch *et al.*, 2009; Mattila *et al.*, 2009, 2012). It is unknown whether protein sorting in the ARE occurs via mechanisms that are the same as or distinct from those in the TGN.

The neurotrophin receptor p75 is an apically sorted transmembrane protein that does not associate with lipid rafts along the biosynthetic pathway (Breuza *et al.*, 2002; Delacour *et al.*, 2007). Disruption of the single N-linked glycosylation site on p75 has no effect on apical sorting, whereas deletion of the entire or membrane-proximal portion of the heavily O-glycosylated stalk domain of p75 impairs polarized delivery (Yeaman *et al.*, 1997; Breuza *et al.*, 2002). Alteration of the spacing between the stalk and the transmembrane domain by addition of two amino acids also redirects p75 to the basolateral surface (Yeaman *et al.*, 1997). Based on these results, it has been hypothesized that the stalk either serves as a signal for lectin binding or acts as a structural prop required to maintain a transport-competent conformation (Rodriguez-Boulan and Gonzalez, 1999). In support of the latter idea, Jacob and colleagues demonstrated that p75 binds to galectin-3 (Gal-3; a member of the galectin family capable of linking glycoproteins into arrays [Delacour *et al.*, 2006; Di Lella *et al.*, 2011]) and that Gal-3 knockdown inhibits apical sorting of p75. Subsequent experiments showed that Gal-3 mediates the transient formation of large oligomers of p75 starting 10 min after release from the TGN (Delacour *et al.*, 2007, 2009), and that Gal-3 likely encounters p75 and other cargoes in apical endocytic compartments (Schneider *et al.*, 2010).

The post-TGN Gal-3–mediated sorting of p75 leaves open the question of how p75 is segregated from other proteins in the TGN. TGN export of p75 is known to occur in carriers distinct from those carrying basolateral proteins and apically destined lipid raft–associated proteins (Kreitzer *et al.*, 2000; Guerriero *et al.*, 2008). We and others have suggested that independent clustering of raft-associated and raft-independent proteins is involved in protein sorting (Paladino *et al.*, 2004, 2007; Lebreton *et al.*, 2008; Weisz and Rodriguez-Boulan, 2009). Thus we asked whether p75 forms higher-order oligomers (hereafter referred to as *clusters*) in the TGN and whether clustering is important for apical targeting. Additionally, we tested whether dimerization of p75 contributes to clustering and apical sorting. Like many apically destined proteins, p75 is known to form dimers, and two regions within the transmembrane domain responsible for dimerization were recently identified (Vilar *et al.*, 2009b). However, the role of the dimerization motif in apical targeting has not been assessed.

Recent technological advances in fluorescence fluctuation measurements, such as photon-counting histogram (PCH) analysis, make it possible to measure protein size and dynamics in live cells on microsecond timescales at single-molecule sensitivity (Chen *et al.*, 2002; Slaughter and Li, 2010). The application of PCH analysis to measure the number and brightness of particles in live cells was formalized originally by Chen and colleagues and further expanded by Mueller (Chen *et al.*, 1999, 2002; Perroud *et al.*, 2003; Macdonald *et al.*, 2013). In PCH, the ratio of variance to intensity of the fluorescence signal is measured to determine the molecular brightness of molecules diffusing through a small confocal volume. For example, the fluorescence intensity of a 4 nM solution of monomer protein is the same as 1 nM of tetramer, but the variance and therefore the brightness of the tetramer signal is expected to be fourfold greater (Supplemental Figure S1A). This powerful technique, which requires very low protein expression, has been used to measure the oligomeric status of several membrane proteins, including glycosylphosphatidylinositol (GPI)-anchored proteins, G protein–coupled receptors (GPCRs), and a hormone receptor (Malengo *et al.*, 2008; Wolf-Ringwall *et al.*, 2011; Herrick-Davis *et al.*, 2012). PCH measurements are performed at discrete spots in the cell, which makes PCH technically cumbersome to use for determining spatial variation in protein size, because a large number of individual measurements are required. However, the imaging analogue of PCH analysis, called number and brightness (N&B) analysis and developed by Digman and colleagues, can assess the spatial variation in oligomeric status (Digman *et al.*, 2008).

In this study, we used PCH, N&B analysis, imaging, and biochemical approaches to assess the role of p75 domains in clustering and apical sorting. Our data suggest that transient clustering is necessary but not sufficient for apical sorting of p75 in the TGN and shed new light on the mechanism of apical sorting of raft-independent proteins and on how sorting hierarchies are interpreted within the biosynthetic pathway.

## RESULTS

### Inhibition of p75 dimerization impairs apical sorting

The membrane-proximal O-glycosylated stalk of p75 is required for efficient targeting of p75 to the apical surface of polarized epithelial cells. (Le Bivic *et al.*, 1991; Yeaman *et al.*, 1997). Recently Vilar and colleagues identified two regions within the transmembrane region of p75 (Cys-257 and AlaxxxGly-266) that are required for dimerization of p75 (Vilar *et al.*, 2009b). Mutation at both sites (C257A/G266I; see Figure 1 for a schematic of all constructs used) disrupted dimer formation and impaired some but not all p75-dependent signaling pathways in neuronal cells (Vilar *et al.*, 2009b). To test whether dimerization is important for the polarized sorting of p75, we generated Madin-Darby canine kidney (MDCK) cell lines stably expressing either wild-type p75 or p75 with C257A/G266I mutations. Electrophoresis of wild-type p75 under nonreducing conditions confirmed dimer formation with similar efficiency to that observed by others (6.9 ± 0.9%; Figure 2A; Vilar *et al.*, 2009b; Sykes *et al.*, 2012). In contrast, only 0.8 ± 0.3% of the

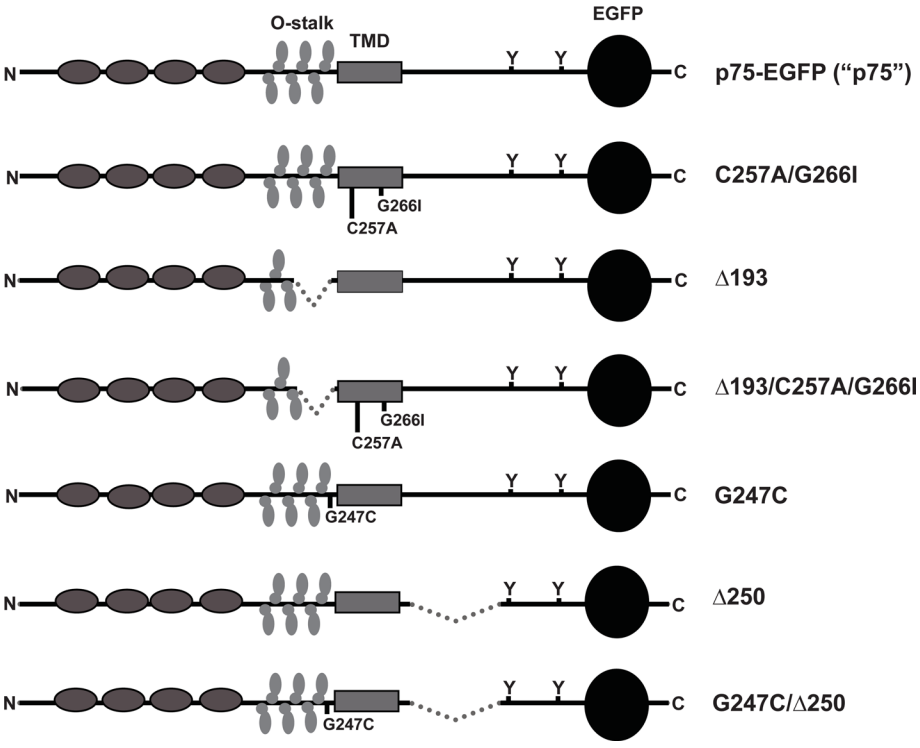


FIGURE 1: Schematic of wild-type and mutant p75 proteins. The domain structure of wild-type and mutant mEGFP-tagged p75 proteins is shown. Gray ovals represent cysteine-rich repeats, vertical ovals represent O-glycosylation within the juxtamembrane stalk (O-stalk), the solid gray rectangle represents the transmembrane domain, Ys represent the cytoplasmic tyrosine residues at positions 308 and 340 (numbering based on mature human form), and the black circle represents mEGFP. Wild-type p75-EGFP is referred to throughout the manuscript as p75; C257A/G266I, mutation of cysteine and glycine (important for dimer formation) to alanine and isoleucine at positions 257 and 261, respectively; Δ193, deletion of amino acids 193–218 of the O-stalk (important for apical sorting); Δ193/C257A/G266I, combination of Δ193 and C257A/G266I mutations; G247C, mutation of glycine at position 247 to cysteine (enhances dimer formation); Δ250, deletion in cytoplasmic tail of amino acids 250–306 (enhances basolateral sorting); G247C/Δ250, combination of Δ250 and G247C mutations.

C257A/G266I mutant protein formed dimers (Figure 2A). To test whether disruption of dimerization impacted apical targeting, we used confocal microscopy to examine the distribution of fluorescently tagged wild-type and mutant p75 in polarized MDCK cells. Whereas wild-type p75 was detected almost exclusively at the apical surface, the C257A/G266I mutant was partially mislocalized to the basolateral surface of polarized MDCK cells (Figure 2B). To confirm that this mislocalization reflected aberrant sorting of newly synthesized p75, we radiolabeled cells for 2 h and then performed domain-selective biotinylation to quantify polarized delivery. As shown in Figure 2, C and D, whereas 68.9 ± 2.7% of wild-type protein was delivered apically, membrane targeting of the C257A/G266I mutant was nonpolarized (48 ± 2.2%; $p = 0.00024$). Deletion of the membrane-proximal region of the O-glycosylated stalk of p75 (Δ193; Figure 1) did not affect dimerization (Figure 2A) but disrupted apical sorting (53.6 ± 3.4%; Figure 2, C and D). While the polarity we observed for this mutant is similar to that reported in (Delacour *et al.*, 2007), the original description of this mutant suggested a more severe defect in sorting (Breuza *et al.*, 2002); the reason for this variation in sorting efficiency is not known. Combined mutation of both the dimerization motif and the stalk (Δ193/C257A/G266I; Figure 1) did not enhance missorting compared with the individual mutations, suggesting these motifs do not act synergistically (Figure 2, C and D).

**p75 forms transient clusters in the TGN**

Previous studies suggested that clustering of lipid raft–associated proteins in the TGN is required for apical sorting of proteins (Zurzolo *et al.*, 1994; Paladino *et al.*, 2004, 2007; Lebreton *et al.*, 2008). To test whether this is also true for raft-independent proteins, we used PCH analysis to assess p75 clustering in living cells. This technique enables us to quantitate the average brightness of moving fluorescent particles measured within a very small confocal volume over a rapid timescale and can be used to extrapolate the average number of fluorescent proteins that are diffusing together. As controls, we compared the average brightness of enhanced green fluorescent protein (EGFP) expressed in the cytosol of transfected MDCK cells with that of a tandem construct of two EGFP proteins linked together (t-EGFP; Figure 3A). As predicted, t-EGFP was approximately twice as bright compared with monomeric EGFP (Chen *et al.*, 2002; Slaughter *et al.*, 2007, 2008). Stable cell lines expressing wild-type or p75 mutants were incubated at 19ºC to stage proteins in the TGN, and their molecular brightness was measured. We coexpressed the TGN marker GalT-mCherry to aid in selecting the pool of p75 residing in this compartment (Figure S1B). Wild-type p75 measurements at the TGN were heterogeneous, with brightnesses ranging from one to five EGFP molecules per complex, suggesting that p75 clusters exist in the TGN (Figure 3B). Importantly, we obtained a similar range of values in polarized cells grown on coverslips, suggesting that cell differentiation, metabolic state, and density did not influence the level of p75 clustering (Figure 3B). The heterogeneity we observed may be due in part to selective bleaching of larger, slowly moving clusters. Alternatively or in addition, only a subset of p75 in the TGN may be present in large clusters at any given time, or there may be variable numbers of fluorescently tagged p75 molecules incorporated into larger protein complexes that contain other nonfluorescent cargoes.

In contrast to the clustering we observed in the TGN, most of the p75 measured at the plasma membrane had a brightness approaching that of t-EGFP (median 1.71 ± 0.15), suggesting the predominant species is a dimer (Figure 3B), in agreement with previous studies using alternative methods (Vilar *et al.*, 2009b; Sykes *et al.*, 2012). Thus clustering of p75 appears to occur transiently during passage through the biosynthetic pathway.

We next assessed whether clustering of p75 correlates with apical sorting. In contrast to wild-type p75, mutants lacking the dimerization motif and/or stalk did not form clusters. As predicted from our dimerization analysis in Figure 2, the C257A/G266I and Δ193/C257A/G266I mutants had an average brightness close to one (similar to that of monomeric EGFP), confirming a defect in dimerization (Figure 3B). In contrast, mutation of only the O-glycosylated stalk (Δ193) did not disrupt dimerization (median brightness of 1.67 ± 0.24) but impaired higher-order clustering (Figure 3B).

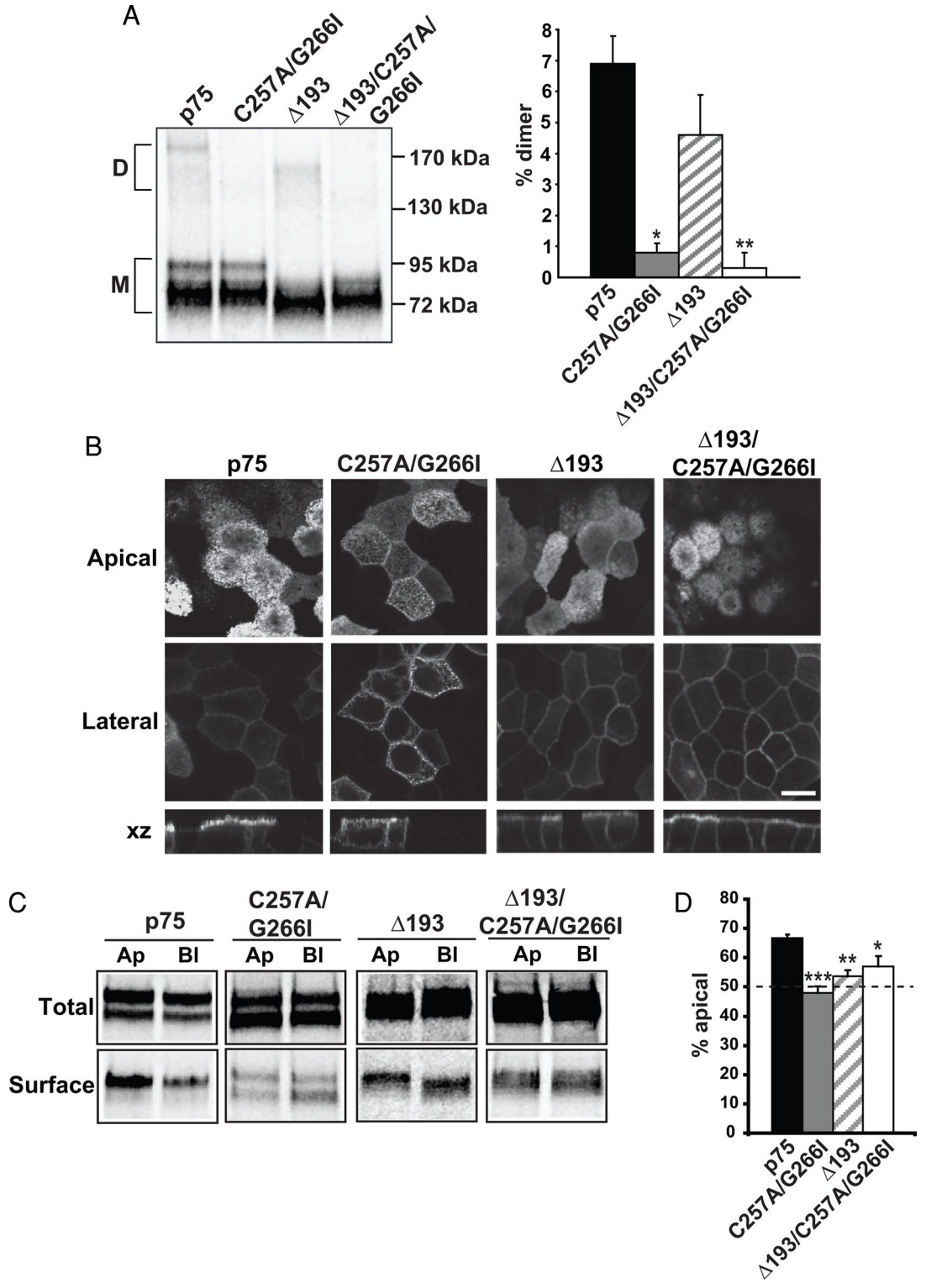


FIGURE 2: Disrupting dimerization reduces p75 apical sorting efficiency. (A) MDCK cells expressing p75 or the C257A/G266I, Δ193, and Δ193/C257A/G266I mutants were radiolabeled for 2 h and then solubilized, and p75 proteins were immunoprecipitated and analyzed by PAGE under nonreducing conditions. A representative gel is shown with the migration of molecular mass standards indicated on the right (D, dimer; M, monomer). Results of three experiments performed in duplicate or triplicate are plotted (mean ± SEM). Unpaired *t* test: *, $p < 0.001$ (p75 vs.C257A/G266I); **, $p < 0.001$ (p75 vs. Δ193/C257A/G266I). (B) Fluorescence images of MDCK cells stably expressing p75, C257A/G266I, Δ193, and Δ193/C257A/G266I mutants. Apical, lateral, and *xz* images from a confocal stack are shown. Scale bar: 10 μm. (C) Domain-selective biotinylation of radiolabeled p75, C257A/G266I, Δ193, and Δ193/C257A/G266I mutants. A representative gel is shown. Ap, apical; Bl, basolateral; Total, one-fifth of total labeled protein. (D) Quantitation of three to five experiments, each performed in duplicate, is plotted as the percent of total labeled protein biotinylated at the apical surface. Unpaired *t* test: ***, $p < 0.001$; **, $p < 0.01$; *, $p < 0.05$.

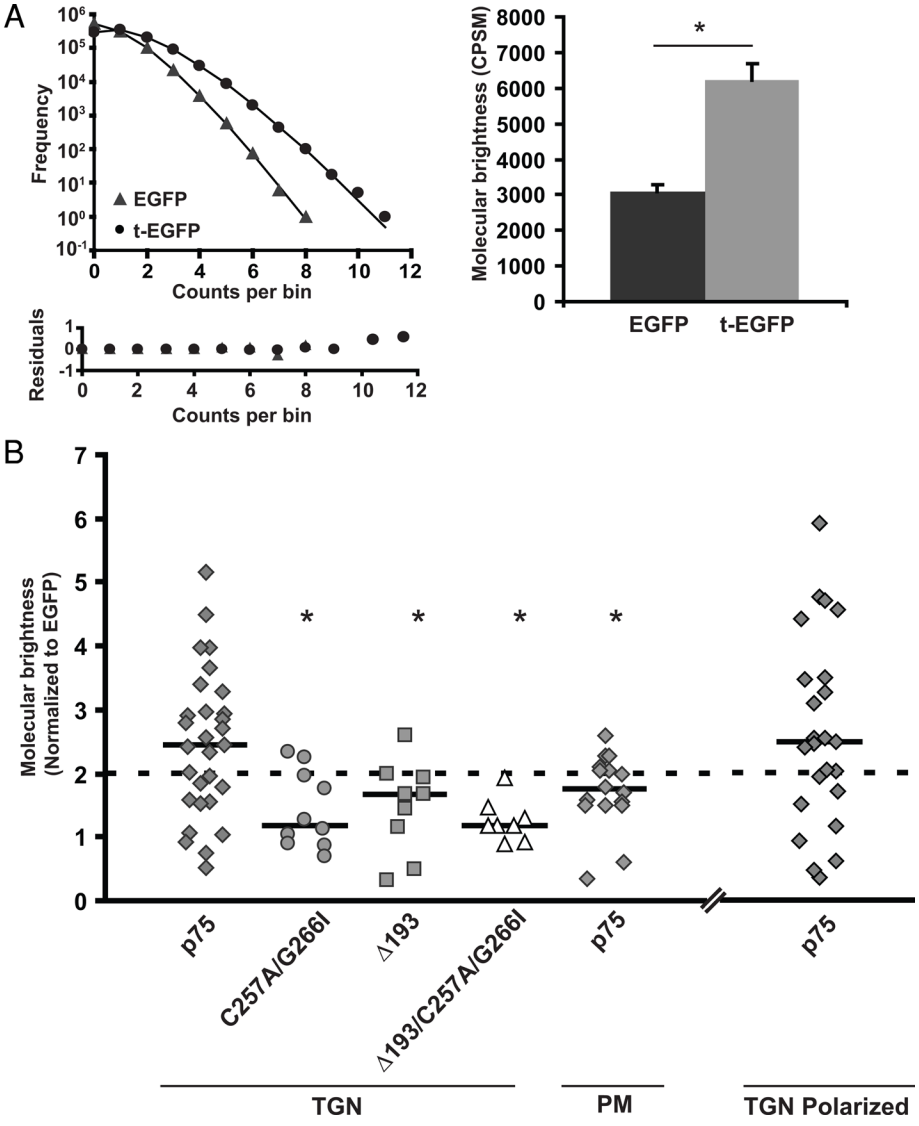


FIGURE 3: p75 but not missorted mutants transiently form clusters in the TGN. (A) Representative PCHs for EGFP (triangle) and t-EGFP (circle) proteins. Bottom, residuals for fit of histograms. Histograms were fitted as described in *Materials and Methods* to obtain molecular brightness expressed as counts per second per molecule for EGFP ($n = 20$) and t-EGFP ($n = 18$). *, $p < 0.001$. (B) PCH plot normalized to brightness of EGFP for measurements of p75 in the TGN ($n = 29$; diamonds); C257A/G266I ($n = 10$; circles); Δ193 ($n = 9$; squares); Δ193/C257A/G266I ($n = 8$; triangles), and p75 at the plasma membrane ($n = 15$; diamonds); p75 in the TGN of polarized cells ($n = 24$, diamonds). The dotted line corresponds to molecular brightness of a dimer (t-EGFP). Solid horizontal lines show the median brightness for each sample. Unpaired *t* test: *, $p < 0.05$ compared with p75 in the TGN.

In a related approach to confirm selective clustering of wild-type p75, we used an imaging analogue of PCH analysis, N&B analysis. This technique can spatially map the molecular brightness of fluorescent proteins in living cells without the significant bleaching of slowly diffusing membrane proteins that can occur with PCH measurements. We compared the molecular brightness of wild-type p75 and the Δ193/C257A/G266I mutant staged in the TGN. Using this approach, we calculated an average molecular brightness for wild-type p75 at the TGN of 8.8 ± 2.1 molecules per oligomer. In contrast, clustering was greatly reduced for the Δ193/C257A/G266I mutant (2.9 ± 0.4). Importantly, using N&B, we could detect differences in the brightness of p75 within subregions of the TGN (Figure 4A). For example, higher average brightness of p75 was measured in the periphery compared with the center of the TGN, demonstrating spatial differences in clustering (10.4 ± 2.4 vs. 6.9 ± 1.7, respectively; Figure 4B). The higher average value for p75 clustering we obtained using this approach compared with the trend seen by PCH suggests that bleaching may contribute to the reduced average cluster sizes we observed using PCH. Together these results demonstrate for the first time that p75 forms spatially heterogeneous clusters in the TGN of living cells and identify a previously unknown requirement for dimerization in the formation of p75 clusters and in apical sorting.

### O-glycosylation of p75 does not play a direct role in apical sorting

Our data suggest that dimerization and the O-glycosylated stalk of p75 are both required for formation of higher-order clusters, as well as for apical sorting. Noncovalent interactions of p75 dimers with adjacent proteins via the stalk or another domain could mediate formation of higher-order p75 clusters. Alternatively, p75 could be cross-linked into clusters via *O*-glycan binding to Gal-3 or other galectins (Delacour *et al.*, 2007). To begin to distinguish between these possibilities, we assessed the role of p75 O-glycosylation and galectin expression in p75 sorting.

The structure of *O*-glycans on p75 expressed in MDCK cells is not known. Gal-3 preferentially binds to polylactosamine (PL) extensions comprising repeating units of Galβ1-4GlcNAcβ1-3 on N- and O-linked glycans (Knibbs *et al.*, 1993; Stowell *et al.*, 2008; Poland *et al.*, 2011). To determine whether p75 glycans contain PL extensions, we incubated immunoprecipitated radiolabeled p75 with beads conjugated to *Lycopersicon esculentum* agglutinin (LEA) lectin, which selectively recognizes PL. Only 4% of total p75 was recovered on these beads, suggesting there is little to no PL on p75 glycans when the protein is expressed in MDCK cells (unpublished data). Moreover, there was no decrease in binding to LEA beads when p75 was synthesized in cells overexpressing the sialyltransferase ST6GalNAc-1 (ST6), which prevents PL addition to O-linked glycans (Sewell *et al.*, 2006; Kinlough *et al.*, 2011). In contrast, ~25% of the transmembrane mucin MUC1 expressed in MDCK cells was recovered on LEA beads, and binding was reduced to ~8% when MUC1 was expressed in ST6 cells (Kinlough *et al.*, 2011; Rebecca Hughey, personal communication). These data suggest that, unlike MUC1, *O*-glycans on p75 are not normally modified by PL extension. The steady-state distribution of p75 expressed in ST6 versus MDCK cells was identical as assessed by immunofluorescence (Figure 5A). Similarly, using domain-selective biotinylation we found no difference in the polarized delivery of newly synthesized p75 expressed in ST6 versus parental MDCK cells (73 ± 0.5% vs. 74 ± 3.2% apical, respectively; Figure 5B).

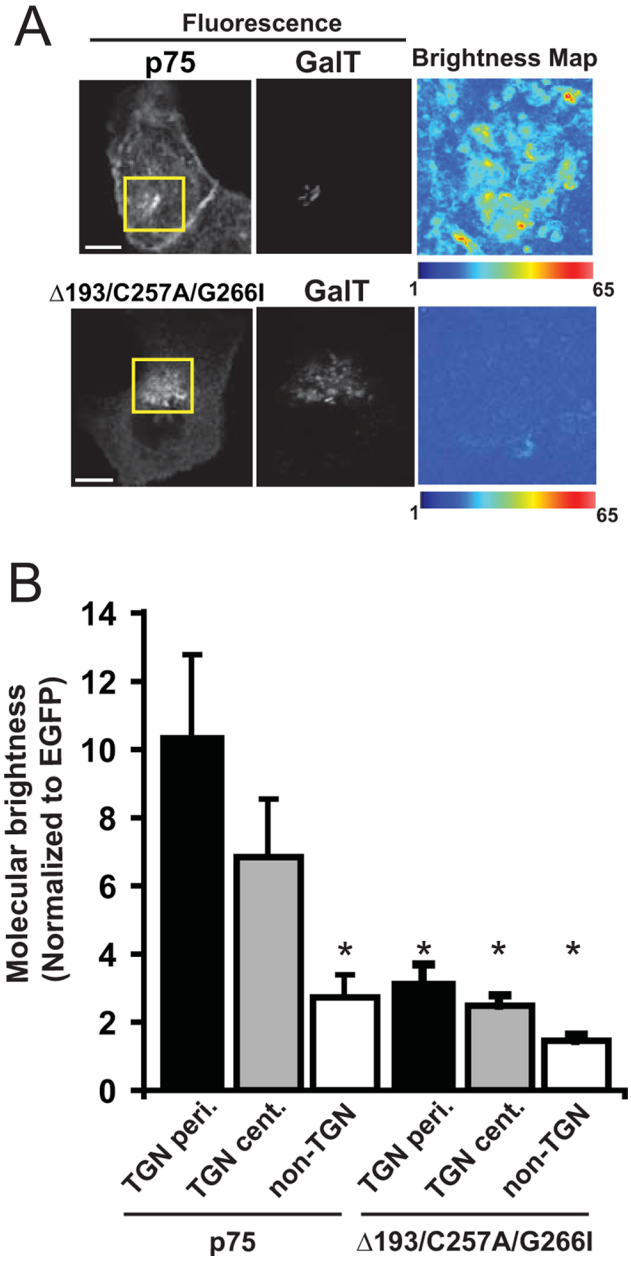


FIGURE 4: p75 clustering is spatially heterogeneous at the TGN as measured by N&B analysis. (A) Wild-type p75 and the Δ193/C257A/G266I mutant were staged at the TGN of MDCK cells coexpressing the TGN marker GalT-mCherry as described in *Materials and Methods*. Left, fluorescence images showing staging of wild-type and mutant p75 in the TGN. Scale bar: 10 μm. Right, map of molecular brightness for the inset regions shown in the fluorescence images. Scale = normalized molecular brightness (× EGFP) per pixel. Note the heterogeneity in brightnesses. (B) Brightness values normalized to EGFP for measurements of p75 and Δ193/C257A/G266I in the periphery of the TGN (TGN-peri; $n = 12$ and 7, respectively), in the center of the TGN (TGN-cent.; $n = 11$ and 4, respectively), and in non-TGN regions ($n = 12$ and 7, respectively). Unpaired *t* test: *, $p < 0.05$ compared with p75 in the TGN-peri. Average brightness calculated for the entire TGN was 8.8 ± 2.1 for p75 and 2.9 ± 0.4 for Δ193/C257A/G266I. Unpaired *t* test: *, $p < 0.05$ compared with p75 in TGN-peri.

As an additional test for glycan-dependent sorting of p75, we knocked down Gal-3, Gal-4, and Gal-9 in MDCK cells and examined the effect on apical targeting of p75 by immunofluorescence. Knockdown efficiency of each small interfering RNA (siRNA) was assessed by reverse transcriptase-PCR (RT-PCR; Figure 5E) and ranged between 60 and 90%. As shown in Figure 5C, depletion of all three galectins simultaneously had no effect on p75 polarity as assessed by immunofluorescence. Domain-selective biotinylation confirmed there were no subtle alterations in polarized delivery of p75 in control versus galectin knockdown cells (75 ± 0.7 vs. 73 ± 1.7% apical, respectively; Figure 5D). Similarly, we found no effect on p75 polarity of depleting the galectins individually (unpublished data). These findings are consistent with our previously published studies showing no effect of Gal-3 or Gal-9 knockdown on p75 delivery or steady-state distribution (Mo *et al.*, 2010, 2012). Together these data suggest that 1) glycans on p75 expressed in MDCK cells do not contain significant amounts of PL; 2) alterations to *O*-glycan structures on p75 by overexpression of ST6 do not affect polarized delivery of the protein; and 3) the primary galectins expressed in MDCK cells do not play a role in polarized sorting of p75. We conclude from these results that the O-glycosylated stalk plays a structural role in the formation of p75 clusters in the TGN and that galectins are not involved in this process.

### Enhancement of dimerization restores clustering but not apical sorting to a basolaterally directed mutant of p75

To determine whether clustering and polarity are directly linked, we asked whether a basolaterally sorted mutant of p75 that retains an intact dimerization motif and stalk domain forms clusters in the TGN. Previous studies have shown that deletion of ~60 amino acids within the cytosolic tail of p75 (Δ250, Figure 1) positions two tyrosine residues closer to the transmembrane region and greatly enhances their function as basolateral sorting signals (Le Bivic *et al.*, 1991). We confirmed by immunofluorescence and domain-selective biotinylation of stably expressing MDCK cells that the Δ250 mutant sorts strongly to the basolateral surface (24 ± 6.0% apical; Figure 6, B–D). As expected, dimerization of the Δ250 mutant was similar to that of wild-type p75 (Figure 6A). Strikingly, however, clustering of Δ250 as assessed by PCH analysis was significantly impaired compared with wild-type p75, even though the transmembrane and lumenal domains of p75 are intact in this mutant (Figure 6E). Together these data suggest that the presence of dominant basolateral sorting information in Δ250 prevents p75 clustering.

Finally, we asked whether artificially enhancing dimerization could increase clustering and apical sorting of either wild-type p75 or the Δ250 mutant. To this end, we mutated Gly-247 within the stalk domain of wild-type p75 or Δ250 to cysteine (G247C and G247C/Δ250; Figure 1) and generated MDCK cell lines stably expressing these constructs. The G247C mutation has been shown previously to enhance p75 dimerization (Vilar *et al.*, 2009a). SDS–PAGE under nonreducing conditions confirmed that recovery of dimers of both G247C and G247C/Δ250 was dramatically increased compared with wild-type p75 (Figure 6A). Whereas 29 ± 1.4% of G247C was recovered as a dimer (compared with 5.8 ± 3.5% of wild-type p75), we reproducibly observed even greater dimerization efficiency for the G247C/Δ250 mutant (56 ± 4.2% dimerized); the reason for this is unclear.

Both polarity and clustering of the G247C mutant were similar to wild-type p75 as assessed by domain-selective biotinylation and PCH analysis (Figure 6, C–E), suggesting that enhanced dimerization does not affect either clustering or apical sorting efficiency of p75. However, addition of the G247C mutation did significantly increase clustering in the context of the Δ250 deletion (G247C/Δ250, Figure 5E). Nonetheless, the polarity of

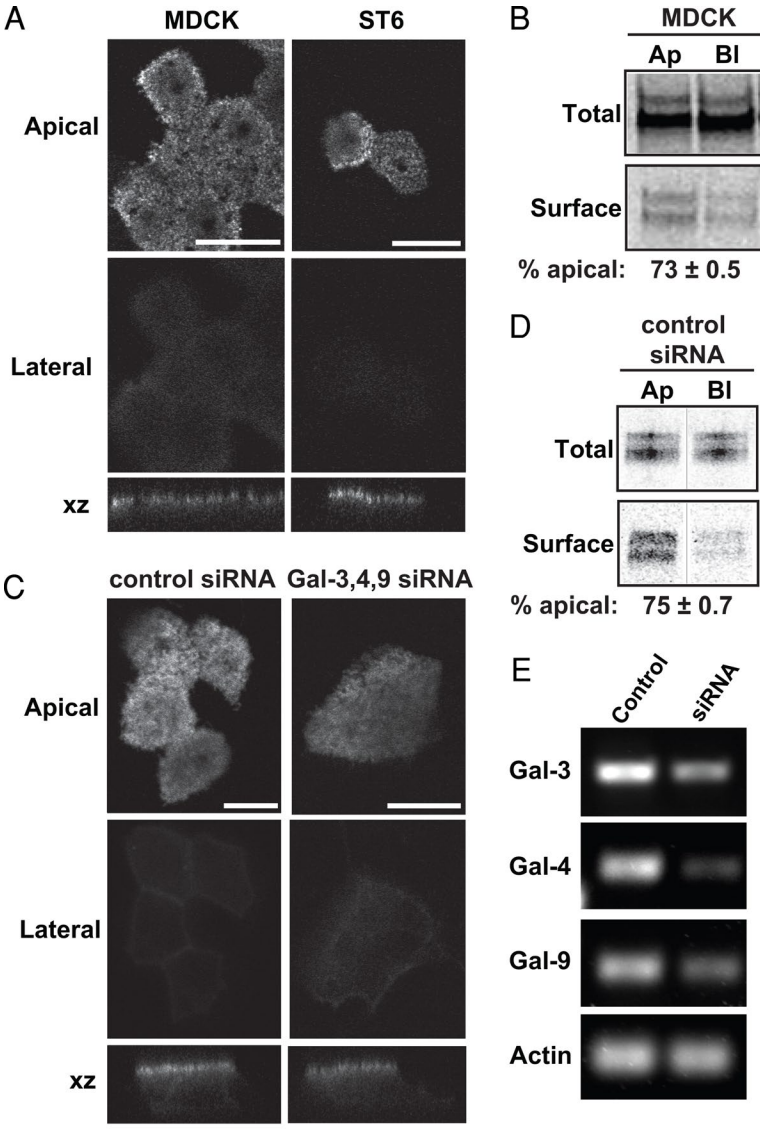


FIGURE 5: Neither PL extension on p75 *O*-glycans or galectins are required for efficient apical sorting of p75. (A) Polarized MDCK cells stably expressing the sialyltransferase ST6 (which disrupts formation of PL extensions) or parental MDCK cells were infected with adenovirus encoding p75 and processed the following day for confocal microscopy. Apical, lateral, and *xz* sections are shown. Scale bar: 10 μm. (B) ST6 and parental cells expressing p75 were radiolabeled and biotinylated as described in *Materials and Methods*. Representative gels showing total and biotinylated protein are shown, and the polarity assessed in two independent experiments is noted below. Ap, apical; Bl, basolateral; Total, one-fifth of total labeled protein. (C) Fluorescence images of polarized p75-expressing MDCK cells transfected with control siRNA or a mixture of siRNAs targeting Gal-3, Gal-4, and Gal-9. Images of apical, lateral, and *xz* sections are shown. Scale bars: 5 μm for control; 10 μm for knockdown. (D) Biotinylation of p75 was performed as described above. Representative gels showing total and biotinylated protein are shown, and the polarity assessed in two independent experiments is noted below. (E) Knockdown efficiency of each galectin was assessed by RT-PCR. A representative gel is shown with β-actin amplified as a loading control. Knockdown efficiency was ~60–70% for Gal-3, >90% for Gal-4, and ~90% for Gal-9.

the G247C/Δ250 mutant was similar to that of the Δ250 mutant alone (Figure 6, B–D). Thus, artificially restoring cluster formation is insufficient to overcome strong basolateral sorting information to divert Δ250 to the apical surface. The implications of this result with respect to the hierarchy of polarized sorting decisions are discussed below.

## DISCUSSION

In the present study, we have identified a role for dimerization and formation of higher-order clusters in the efficient sorting of p75 to the apical surface of polarized renal epithelial cells. We found that wild-type p75 formed clusters in the TGN but not at the plasma membrane of MDCK cells. Mutation of the dimerization motif in the transmembrane domain disrupted apical sorting and also abrogated clustering of p75. Another missorted mutant of p75 lacking part of its O-glycosylated stalk formed dimers but was also unable to cluster. Strikingly, a second missorted p75 mutant with strong cytoplasmic basolateral sorting information but intact dimerization and stalk motifs formed dimers but did not cluster. Enhancing the dimerization of this mutant restored clustering but did not result in apical targeting. Together our data suggest that p75 dimerization and clustering are necessary but not sufficient for efficient sorting to the apical surface. Moreover, our studies begin to explain mechanistically how a hierarchy of sorting decisions directs p75 and mutants to distinct domains in polarized cells.

### p75 clustering in living cells

The use of PCH and N&B analyses enabled us to detect p75 clusters at high temporal (microsecond) and spatial resolution in living cells. The cluster sizes we measured were variable but on average quite low (~3) based on PCH analysis. However, we noted that some bleaching occurred during PCH measurements, which can lead to underestimates of brightness. This, together with the potential for spatial heterogeneities in clustering, could contribute to the variability in cluster size. We used N&B analysis as an alternative approach to examine p75 clustering, because there is minimal bleaching in this technique and spatial heterogeneities in brightness can be mapped. Our N&B analysis confirmed that p75 clusters in the TGN, and using this method, we observed an average value of 8.8 fluorescent molecules per cluster. Similar to our results using PCH analysis, there was a broad range in brightness values of p75 in the TGN. Importantly, using N&B analysis, we were able to observe spatial heterogeneity in p75 cluster size, which may reflect the segregation of p75 clusters into microdomains, possibly TGN export sites.

Several other groups have previously attempted to measure the extent and location of p75 clustering with conflicting results (Breuza *et al.*, 2002; Delacour *et al.*, 2007; Lebreton *et al.*, 2008; Vilar *et al.*, 2009b). No clustering of p75 was detected on velocity-sedimentation gradients (Breuza *et al.*, 2002; Paladino *et al.*, 2007) or by fluorescence recovery after photobleaching (FRAP; Lebreton *et al.*, 2008).

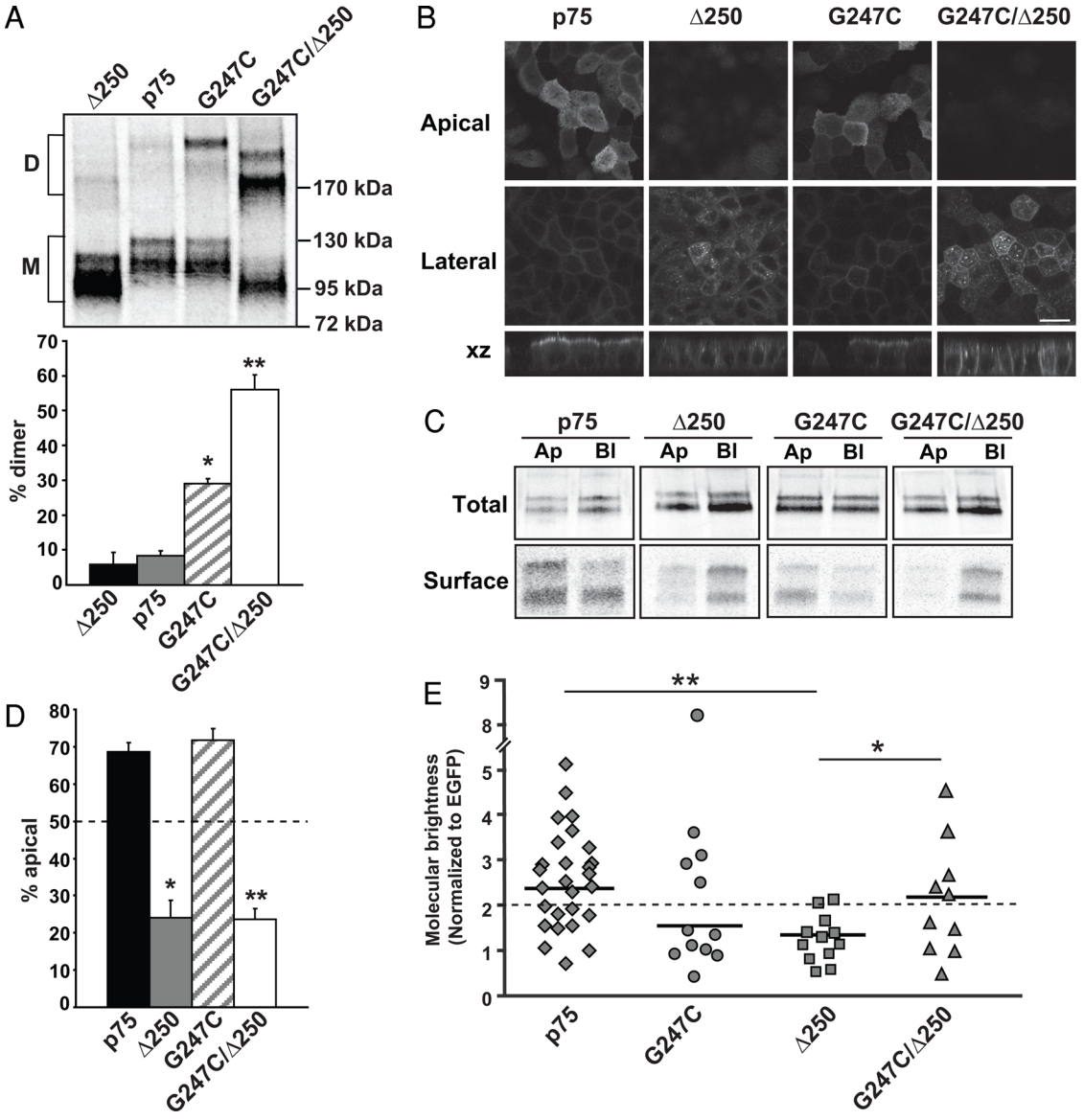


FIGURE 6: A basolaterally sorted p75 mutant does not cluster, and artificial clustering does not restore apical sorting. (A) Nonreducing gel electrophoresis of wild-type p75 and the G247C, Δ250, and G247C/Δ250 mutants. A representative gel is shown and the migration of dimers (denoted as "D") and monomers (M) is marked. Quantitation of dimerization efficiency in three experiments performed in triplicate (mean ± SEM) is plotted below. Unpaired *t* test: *, $p < 0.001$ (p75 vs. G247C); **, $p < 0.001$ (p75 vs. G247C/Δ250). (B) Fluorescence images of MDCK cells stably expressing p75, Δ250, G247C, and G247C/Δ250. Cells were seeded on permeable supports and grown for 4 d, fixed, and mounted. Apical, lateral, and *xz* images from a confocal stack are shown. Scale bar: 15 μm. (C) Domain-selective biotinylation of p75 and Δ250, G247C, and G247C/Δ250 mutants. Representative gels showing total and biotinylated protein are shown. Ap, apical; Bl, basolateral; Total, one-fifth of total labeled protein. (D) Quantitation of biotinylation experiments (p75, G247C, and G247C/Δ250, $n = 5$; Δ250, $n = 2$) each performed in duplicate is plotted. Unpaired *t* test: *, $p < 0.05$ (p75 vs. Δ250); **, $p < 0.001$ (p75 vs. G247C/ Δ250). (E) PCH analysis of G247C ($n = 12$, diamonds), G247C/Δ250 ($n = 10$, circles), and Δ250 ($n = 11$, triangles). Data for wild-type p75 (diamonds) are duplicated from Figure 3B for ease of comparison. The dotted line corresponds to molecular brightness of a dimer (t-EGFP). Solid horizontal lines indicate the median brightness of each protein. Unpaired *t* test: *, $p < 0.05$ (Δ250 vs. G247C/Δ250); **, $p < 0.01$ (p75 vs. Δ250).

However, Delacour and colleagues found by using Nycodenz gradient sedimentation that p75 clusters shortly after leaving the TGN and clustering required the p75 stalk domain (Delacour *et al.*, 2007).

Several important considerations might explain the inability to observe p75 clustering in previous studies. First, the dynamic nature of oligomer formation is now appreciated based on recent observations of rapid conversion of oligomeric states of several GPCRs on millisecond to second timescales in live cells (Hern *et al.*, 2010; Kasai *et al.*, 2011; Calebiro *et al.*, 2013). We have observed that stringent lysis and immunoprecipitation procedures must be followed to measure consistent levels of p75 dimers in vitro. The levels of dimerization reported for p75 range from a few percent to 50%, partly due to expression level (Vilar *et al.*, 2009a,b; Sykes *et al.*, 2012). These results, coupled with the heterogeneity of our brightness measurements, suggest that p75 dimerization and clustering are both highly dynamic processes. Moreover, clustering is spatially regulated, as we observed clustering

only in the TGN and not at the plasma membrane. This is consistent with the observations of Vilar and colleagues, who failed to detect clusters of p75 in whole cells using fluorescence anisotropy imaging microscopy (Vilar *et al.*, 2009b). Thus it is not surprising that p75 oligomers would be difficult to observe using in vitro methods that require long centrifugation periods.

A second complication arises in the interpretation of FRAP data to make conclusions regarding oligomeric status. The Saffman-Delbrück model for membrane protein diffusion predicts that a diffusion coefficient is only weakly dependent on the size of a membrane protein (Saffman and Delbrück, 1975), and this has been recently confirmed by Ramadurai and colleagues for a broad range of membrane proteins of different sizes (Ramadurai *et al.*, 2009). Thus diffusion measurements cannot resolve changes in protein size unless these changes are very large (Ramadurai *et al.*, 2009). We encountered this problem when we initially measured the diffusion of wild-type and mutant p75 proteins using fluorescence correlation spectroscopy and detected no significant changes in diffusion (unpublished data). In contrast, PCH and N&B analyses extract brightness information from the fluorescence fluctuations in the amplitude domain and not the time domain, thus they are insensitive to the weak relationship between size and diffusion.

### Role of galectins in apical sorting of p75

Previous studies by Delacour and colleagues found that siRNA knockdown of Gal-3 disrupted both post-Golgi clustering and sorting of p75 and other proteins with glycan-dependent sorting signals (Delacour *et al.*, 2006, 2007). However, our findings here do not support a role for galectins in apical sorting of p75. We found here that glycans on p75 expressed in our MDCK cells have few if any PL extensions and are thus unlikely to bind efficiently to Gal-3. Moreover, knockdown of the three major galectins expressed in MDCK cells had no effect on p75 sorting. While our knockdown efficiency in this study was suboptimal, we have achieved higher efficiency in previous studies (close to 100%) and observed the same result (Mo *et al.*, 2010, 2012). In contrast, several studies, including work from our own laboratory, have suggested roles for galectins in polarized sorting of a variety of other apically destined proteins and lipids (Jacob and Naim, 2001; Stechly *et al.*, 2009; Schneider *et al.*, 2010; Kinlough *et al.*, 2011; Mo *et al.*, 2012). The expanding cellular roles identified for galectins, which include both glycan-dependent and glycan-independent functions, complicate straightforward assessment of these lectins' roles in apical trafficking (Di Lella *et al.*, 2011). Moreover, depletion of Gal-3 or Gal-9 has been suggested to perturb epithelial polarization in general (Koch *et al.*, 2010; Mishra *et al.*, 2010). Regardless, while the role of galectins remains unclear, it is important to stress that no studies have implicated Gal-3 in apical sorting at the TGN, where we observed clustering of p75.

### Hierarchy of signals direct p75 sorting

The apparent absence of a glycan-dependent sorting mechanism for p75 in the TGN leads us to conclude that the dimerization motif and stalk domain play structural roles to precisely orchestrate the formation and dynamics of p75 clustering rather than functioning as ligands for a galectin or other sorting receptor. We hypothesize that p75 dimers assemble into clusters, possibly with other apically destined cargoes, that can provide the avidity to recruit membrane or soluble cellular components required for the formation and targeting of TGN-derived carriers (Figure 7A). TGN export of wild-type p75 has been demonstrated to occur via tubular carriers (Guerriero *et al.*, 2008) that require LIM kinase 1 and dynamin activities followed by KIF-5B–mediated transport to the apical surface (Kreitzer

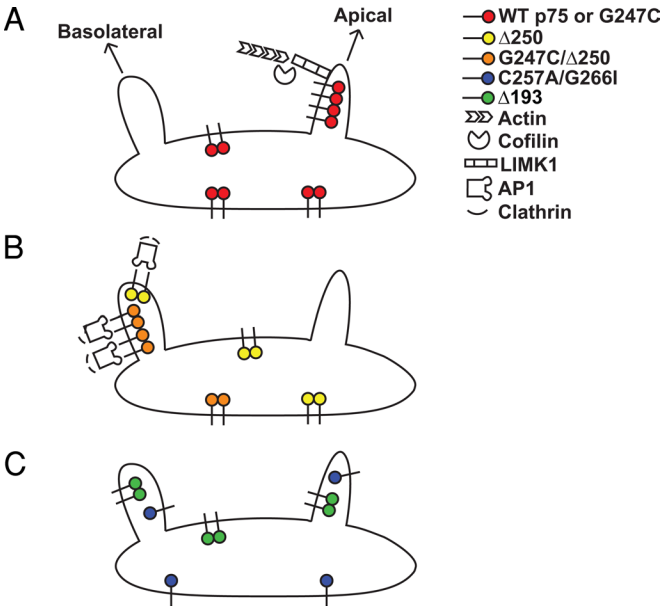


FIGURE 7: Working model for cluster-mediated p75 sorting. (A) Clustering of wild-type p75 (red) enables its segregation into transport carriers that require LIM kinase and cofilin for budding. (B) Deletion of a region of the cytoplasmic tail of p75 in the Δ250 mutant (yellow) creates a dominant basolateral targeting signal and results in AP-1 and clathrin-mediated sorting. Artificial dimerization and clustering of this mutant (G247C/Δ250; orange) does not impede basolateral sorting, suggesting that 1) clustering does not impede basolateral sorting and/or 2) basolateral sorting decisions occur prior to recognition of apical targeting information. (C) Mutation of either the stalk (Δ193; green) or the dimerization motif (C257A/G266I; blue) of p75 prevents clustering and results in nonpolarized surface delivery.

*et al.*, 2000; Jaulin *et al.*, 2007; Salvarezza *et al.*, 2009). None of these components is thought to bind directly to p75. The p75-related protein NRH2 also requires LIM kinase 1 for export (Salvarezza *et al.*, 2009), but whether these cargoes can form coclusters is not known. Introduction of dominant basolateral sorting information in the Δ250 deletion mutant, which moves two YXXΦ motifs closer to the transmembrane domain, prevents clustering, even though the structural elements required for clustering remain intact. Basolateral delivery of proteins with these motifs is thought to be mediated by a pathway dependent on both AP-1 and clathrin (Deborde *et al.*, 2008; Gravotta *et al.*, 2012). Artificially clustering the Δ250 mutant by enhancing its dimerization did not prevent its basolateral targeting; thus clustering per se neither overcomes nor interferes with interpretation of basolateral sorting information (Figure 7B). This is also consistent with a scenario wherein the decision to access a basolateral sorting pathway occurs prior to recognition of any apical sorting information, and may explain why basolateral sorting determinants are frequently dominant over apical targeting signals.

In the context of the above model, what does it mean that impairment of either the dimerization motif or the stalk resulted in nonpolarized (rather than basolateral) delivery? Multiple routes exist from the TGN to both the apical and basolateral surfaces (Jacob and Naim, 2001; Ang *et al.*, 2003; Cresawn *et al.*, 2007; Cramm-Behrens *et al.*, 2008; Desclozeaux *et al.*, 2008; Farr *et al.*, 2009; Folsch *et al.*, 2009; Mattila *et al.*, 2009, 2012). We speculate that p75 mutants that contain no interpretable sorting information (such as Δ193) will randomly access all available pathways to the surface (Figure 6C).

Clustering of raft-associated proteins has been demonstrated to be required for apical sorting in polarized MDCK and other

epithelial cells (Paladino *et al.*, 2004, 2007). Our studies are the first to demonstrate in vivo clustering of raft-independent cargoes and a role for dimerization and higher-order clustering in their apical sorting. Thus transient formation of protein oligomers may represent a universal step along the biosynthetic pathway that enables the segregation and targeting of apically destined proteins into transport carriers. Future studies will be directed toward dissecting the molecular details of how clustering facilitates this process.

## MATERIALS AND METHODS

### Plasmid construction

Dimerization, stalk, and cytoplasmic tail p75 mutants were generated by PCR overlap/extension and site-directed mutagenesis using pN1-p75-EGFP as a template and the appropriate primers listed in Supplemental Table S1. PCR fragments were subcloned into *Kpn*I and *Apa*I sites of pN1-mEGFP. Unless otherwise stated, all p75 proteins tagged with mEGFP are referred to here as p75 or mutant p75. Replication-defective recombinant adenovirus encoding p75-EGFP was generated as described in (Henkel *et al.*, 1998). Addition of a fluorescent protein to the carboxyl-terminus of p75 does not alter the death-signaling activity or apical trafficking of p75 (Kreitzer *et al.*, 2003; Sykes *et al.*, 2012). The tandem mEGFP-mEGFP (tEGFP) construct was generated by PCR amplification of full-length mEGFP from pN1-mEGFP using primers listed in Table S1 and then subcloned into the *Kpn*I and *Apa*I sites of pN1-mEGFP.

### Cell culture

MDCK II cells were grown in Minimum Essential Medium Eagle (Sigma-Aldrich, St. Louis, MO) supplemented with 10% fetal bovine serum (FBS; Gemini Bio-Products, Sacramento, CA). Stable cell lines were generated by transfecting ~$1 \times 10^6$ cells with 2 µg DNA with 4 µl Lipofectamine 2000 (Invitrogen, Carlsbad, CA). Single colonies were selected in G418-containing medium. MDCK cells stably expressing ST6 (Kinlough *et al.*, 2011) were provided by Rebecca Hughey (University of Pittsburgh).

### Immunofluorescence microscopy

MDCK cells stably expressing wild-type p75-mEGFP or p75 mutants were fixed with 4% paraformaldehyde, processed, and mounted as previously described (Mo *et al.*, 2012). In some instances, cells were incubated with monoclonal anti-GFP primary antibody (Invitrogen) and Alexa Fluor 488 goat anti-mouse secondary (Invitrogen-Molecular Probes, Carlsbad, CA) to enhance the fluorescence signal. Image stacks (0.13–0.2 µm) were acquired on a Leica (Wetzlar, Germany) TCS SP microscope or Zeiss (Oberkochen, Germany) 510 LSM microscope and processed using Adobe (San Jose, CA) Photoshop and MetaMorph (Molecular Devices, Sunnyvale, CA).

### Domain-selective biotinylation

MDCK cells were seeded onto Transwell permeable supports (Corning, Lowell, MA) and grown for 4 d. Cells were labeled with EasyTag [$^{35}$S]cysteine/methionine for 2 h and biotinylated as described in (Weisz *et al.*, 1993; Potter *et al.*, 2004), and wild-type and mutant p75 proteins were immunoprecipitated with rabbit anti-GFP antibody (Invitrogen). Precipitated proteins were separated on 4–15% Criterion gradient gels (Bio-Rad, Hercules, CA). Mature p75 protein bands were quantified using Quantity One software (Bio-Rad).

### Nonreducing gel electrophoresis

MDCK cells stably expressing wild-type or mutant p75 constructs were plated on six-well multiwell plates (Benton Dickinson, Franklin Lakes, NJ) for 2 d prior to experiments to achieve a cell density of ~80% confluence, induced with 10 mM butyrate for 21–24 h, incubated in cysteine/methionine-free medium for 30 min, and radiolabeled with 5 µCi/ml EasyTag [$^{35}$S]cysteine/methionine for 2 h. Cells were solubilized in phosphate-buffered saline containing calcium, magnesium, 0.2 mM iodacetamide (freshly added), 1% Triton X-100, 17.5 mg/ml octyl-β-D-glucopyranoside, and protease inhibitors. Lysates containing labeled p75 proteins were precleared with Pansorbin cells, immunoprecipitated with rabbit anti-GFP antibody (Invitrogen) for 2 h (with Pansorbin cells added during the last 30 min), washed three times with RIPA buffer, and resuspended in Laemmli sample buffer lacking reducing agent. Samples were electrophoresed on 4–15% Criterion gradient gels at 200 V with cold running buffer and visualized using a phosphorimager (Bio-Rad). Protein bands were quantified using Quantity One software (Bio-Rad).

### PCH measurements

MDCK II cells were plated on 0.17 mm Delta T Bioptechs live-cell dishes ([1–1.5] × $10^5$ cells/dish; Bioptechs, Butler, PA) and transfected with 200–500 ng of p75 or mutant plasmid in combination with 50 ng GalT-mCherry (to identify the TGN) using Lipofectamine 2000. Growth media was replaced 12–16 h posttransfection with media lacking phenol red and supplemented with 50 µg/ml cycloheximide (TGN staging buffer), and cells were incubated at 19°C for 3–5 h to accumulate p75 or mutant in the TGN. For polarized experiments, cells were allowed to grow for 4–5 d and were then infected with an adenovirus encoding p75-EGFP (25–50 moi) for 6–8 h, after which they were incubated at 19°C to stage protein in the TGN. After TGN staging, cells were transferred to a live-cell chamber (Pathology Devices, Westminister, MD) maintained at 27°C or 37°C with 5% $CO_2$ and 65% humidity. There was no difference in PCH measurements of p75 with EGFP or mEGFP tags, and these data were combined. All measurements for mutants were with mEGFP. Images and PCH measurements were acquired on a Zeiss LSM 510-ConfoCor 3 system equipped with an LD C-Apochromat 40×/1.1 numerical aperture (NA) water objective. For PCH measurements, the 488-nm line of the 20-mW argon laser was attenuated to 0.3% or ~1 µW with an acoustic–optic tunable filter, 488/561 dichroic filter, and 505–540 band-pass emission filter, and the pinhole was set to 70 µm (1 airy unit). Brighter images depicting the site of PCH measurements (TGN or plasma membrane) were acquired with the pinhole set to 3 airy units in order to locate low-expressing cells. TGN staging buffer supplemented with 1% FBS and 2.5 mM 6-hydroxy-2,5,7,8-tetramethylchroman-2-carboxylic acid (Sigma-Aldrich) was used to minimize autofluorescence and bleaching, respectively, during acquisition (Bacia *et al.*, 2006; Cordes *et al.*, 2009). Scans free of significant bleaching and instabilities were used for analysis. Photon counts were collected with 50-µsec bin time during fluorescence correlation spectroscopy (FCS) acquisition and plotted as frequency versus number of photons per bin time. PCHs were fitted by N&B analysis using Zen software installed with PCH module or in Image J using a plug-in developed by Jay Unruh at the Stowers Institute for Medical Research in Kansas City, MO, and originally formalized by Digman *et al.* (2008). The ImageJ plug-in uses Newton's method of nonlinear least-squares to fit to Eq. 1:

$$\langle \varepsilon \rangle = \frac{\sigma^2 - \langle I \rangle}{\gamma \langle I \rangle} = \sum_i f_i \varepsilon_i \qquad (1)$$

where the variable ε represents the average molecular brightness, $\langle I \rangle$ is the intensity of the signal, σ is the variance, *f* is the fractional intensity of species, and γ is the gamma factor that describes the geometric shape of the point-spread function (PSF) and is 0.3536

for one-photon experiments (Thompson, 1991). Cells chosen for PCH analysis had very low fluorescent protein expression to ensure that the confocal volume was not saturated and the PSF had a three-dimensional Gaussian profile. Measurement of the PSF using fluorescently labeled beads confirmed the profile was a three-dimensional Gaussian shape in both the lateral and axial dimensions (unpublished data). Data that displayed signal instabilities, $n > 30$ or fit with $Chi^2 > 2.5$, were not considered in the final PCH analysis.

### N&B measurements

Wild-type or mutant p75 was staged in the TGN as described under *PCH measurements*. One hundred confocal images were acquired on a Leica TCS system equipped with a 63×/1.2 NA water objective with the 488-nm laser attenuated to 2% of output and a 500- to 560-nm emission filter. Images (256 × 256 pixels) were collected at ~1.3-s intervals at 200 Hz using a hybrid detector set in the photon-counting mode. The average molecular brightness (B) and number of particles (N) per pixel were calculated using the SimFCS software (Digman *et al.*, 2008; Laboratory of Fluorescence Dynamics, University of California, Irvine). N and B are defined as

$$N = \frac{\langle k \rangle^2}{\sigma^2} \tag{2}$$

$$B = \frac{\langle k \rangle}{N} = \frac{\sigma^2}{\langle k \rangle} \tag{3}$$

where the variable $k$ represents the signal intensity and $\sigma$ is the variance of the signal. A moving average filter of 10 was used to remove artifacts due to slow cell movements. A 3 × 3 median spatial filter was used to sharpen the N&B map and reduce noise. The molecular brightness of wild-type or mutant p75 was divided by the average brightness of EGFP measured in the cytosol (~5500 cpsm) to obtain the normalized brightness.

### siRNA knockdown and RT-PCR

Galectin knockdown and RT-PCR were performed essentially as described by Mo *et al.* (2010, 2012). Western blotting could not be used to assess the level of galectin knockdown, due to the lack of antibodies that recognize canine galectins. The siRNA sequences targeting Gal-3, Gal-4, and Gal-9 are listed in Table S2. Cells were fixed and mounted for fluorescence microscopy. RNA was extracted from duplicate samples to quantify the extent of knockdown by RT-PCR.

## ACKNOWLEDGMENTS

We thank Rebecca Hughey for MDCK cells stably expressing ST6 and for many helpful discussions and Michelle Digman for helpful discussions on the use of SimFCS for N&B analysis. This study was supported by National Institutes of Health (NIH) grants DK54407 and DK054407-12S1 (to O.A.W.) and DK078734 (to O.B.K.) and by American Heart Association grant 12SDG8960000 (to R.T.Y.). We are grateful for support from the kidney imaging core of the Pittsburgh Center for Kidney Research (P30 DK079307) and from the NIH Technology Center for Network and Pathways grant 8U54GM103529 (salary support to H.T.).

## REFERENCES

Ang AL, Folsch H, Koivisto UM, Pypaert M, Mellman I (2003). The Rab8 GTPase selectively regulates AP-1B-dependent basolateral transport in polarized Madin-Darby canine kidney cells. J Cell Biol 163, 339–350.

Bacia K, Kim SA, Schwille P (2006). Fluorescence cross-correlation spectroscopy in living cells. Nat Methods 3, 83–89.

Breuza L, Garcia M, Delgrossi MH, Le Bivic A (2002). Role of the membrane-proximal O-glycosylation site in sorting of the human receptor for neurotrophins to the apical membrane of MDCK cells. Exp Cell Res 273, 178–186.

Calebiro D, Rieken F, Wagner J, Sungkaworn T, Zabel U, Borzi A, Cocucci E, Zurn A, Lohse MJ (2013). Single-molecule analysis of fluorescently labeled G-protein-coupled receptors reveals complexes with distinct dynamics and organization. Proc Natl Acad Sci USA 110, 743–748.

Cao X, Surma MA, Simons K (2012). Polarized sorting and trafficking in epithelial cells. Cell Res 22, 793–805.

Chen Y, Müller JD, Ruan Q, Gratton E (2002). Molecular brightness characterization of EGFP in vivo by fluorescence fluctuation spectroscopy. Biophys J 82, 133–144.

Chen Y, Müller JD, So PTC, Gratton E (1999). The photon counting histogram in fluorescence fluctuation spectroscopy. Biophys J 77, 553–567.

Cordes T, Vogelsang J, Tinnefeld P (2009). On the mechanism of Trolox as antiblinking and antibleaching reagent. J Am Chem Soc 131, 5018–5019.

Cramm-Behrens CI, Dienst M, Jacob R (2008). Apical cargo traverses endosomal compartments on the passage to the cell surface. Traffic 9, 2206–2220.

Cresawn KO, Potter BA, Oztan A, Guerriero CJ, Ihrke G, Goldenring JR, Apodaca G, Weisz OA (2007). Differential involvement of endocytic compartments in the biosynthetic traffic of apical proteins. EMBO J 26, 3737–3748.

Deborde S, Perret E, Gravotta D, Deora A, Salvarezza S, Schreiner R, Rodriguez-Boulan E (2008). Clathrin is a key regulator of basolateral polarity. Nature 452, 719–723.

Delacour D, Cramm-Behrens CI, Drobecq H, Le Bivic A, Naim HY, Jacob R (2006). Requirement for galectin-3 in apical protein sorting. Curr Biol 16, 408–414.

Delacour D, Greb C, Koch A, Salomonsson E, Leffler H, Le Bivic A, Jacob R (2007). Apical sorting by galectin-3-dependent glycoprotein clustering. Traffic 8, 379–388.

Delacour D, Koch A, Jacob R (2009). The role of galectins in protein trafficking. Traffic 10, 1405–1413.

Desclozeaux M, Venturato J, Wylie FG, Kay JG, Joseph SR, Le HT, Stow JL (2008). Active Rab11 and functional recycling endosome are required for E-cadherin trafficking and lumen formation during epithelial morphogenesis. Am J Physiol Cell Physiol 295, C545–C556.

Digman MA, Dalal R, Horwitz AF, Gratton E (2008). Mapping the number of molecules and brightness in the laser scanning microscope. Biophys J 94, 2320–2332.

Di Lella S, Sundblad V, Cerliani JP, Guardia CM, Estrin DA, Vasta GR, Rabinovich GA (2011). When galectins recognize glycans: from biochemistry to physiology and back again. Biochemistry 50, 7842–7857.

Farr GA, Hull M, Mellman I, Caplan MJ (2009). Membrane proteins follow multiple pathways to the basolateral cell surface in polarized epithelial cells. J Cell Biol 186, 269–282.

Folsch H, Mattila PE, Weisz OA (2009). Taking the scenic route: biosynthetic traffic to the plasma membrane in polarized epithelial cells. Traffic 10, 972–981.

Fuller SD, Bravo R, Simons K (1985). An enzymatic assay reveals that proteins destined for the apical or basolateral domains of an epithelial cell line share the same late Golgi compartments. EMBO J 4, 297–307.

Gravotta D, Carvajal-Gonzalez JM, Mattera R, Deborde S, Banfelder JR, Bonifacino JS, Rodriguez-Boulan E (2012). The clathrin adaptor AP-1A mediates basolateral polarity. Dev Cell 22, 811–823.

Guerriero CJ, Lai Y, Weisz OA (2008). Differential sorting and Golgi export requirements for raft-associated and raft-independent apical proteins along the biosynthetic pathway. J Biol Chem 283, 18040–18047.

Henkel JR, Apodaca G, Altschuler Y, Hardy S, Weisz OA (1998). Selective perturbation of apical membrane traffic by expression of influenza M2, an acid-activated ion channel, in polarized Madin-Darby canine kidney cells. Mol Biol Cell 9, 2477–2490.

Hern JA, Baig AH, Mashanov GI, Birdsall B, Corrie JE, Lazareno S, Molloy JE, Birdsall NJ (2010). Formation and dissociation of M1 muscarinic receptor dimers seen by total internal reflection fluorescence imaging of single molecules. Proc Natl Acad Sci USA 107, 2693–2698.

Herrick-Davis K, Grinde E, Lindsley T, Cowan A, Mazurkiewicz JE (2012). Oligomer size of the serotonin 5-hydroxytryptamine 2C (5-HT2C) receptor revealed by fluorescence correlation spectroscopy with photon counting histogram analysis: evidence for homodimers without monomers or tetramers. J Biol Chem 287, 23604–23614.

Ihrke G, Bruns JR, Luzio JP, Weisz OA (2001). Competing sorting signals guide endolyn along a novel route to lysosomes in MDCK cells. EMBO J 20, 6256–6264.

Jacob R, Naim HY (2001). Apical membrane proteins are transported in distinct vesicular carriers. Curr Biol 11, 1444–1450.

Jaulin F, Xue X, Rodriguez-Boulan E, Kreitzer G (2007). Polarization-dependent selective transport to the apical membrane by KIF5B in MDCK cells. Dev Cell 13, 511–522.
Kasai RS, Suzuki KG, Prossnitz ER, Koyama-Honda I, Nakada C, Fujiwara TK, Kusumi A (2011). Full characterization of GPCR monomer-dimer dynamic equilibrium by single molecule imaging. J Cell Biol 192, 463–480.
Kinlough CL, Poland PA, Gendler SJ, Mattila PE, Mo D, Weisz OA, Hughey RP (2011). Core-glycosylated mucin-like repeats from MUC1 are an apical targeting signal. J Biol Chem 286, 39072–39081.
Knibbs RN, Agrwal N, Wang JL, Goldstein IJ (1993). Carbohydrate-binding protein 35. II. Analysis of the interaction of the recombinant polypeptide with saccharides. J Biol Chem 268, 14940–14947.
Koch A, Poirier F, Jacob R, Delacour D (2010). Galectin-3, a novel centrosome-associated protein, required for epithelial morphogenesis. Mol Biol Cell 21, 219–231.
Kreitzer G, Marmorstein A, Okamoto P, Vallee R, Rodriguez-Boulan E (2000). Kinesin and dynamin are required for post-Golgi transport of a plasma-membrane protein. Nat Cell Biol 2, 125–127.
Kreitzer G, Schmoranzer J, Low SH, Li X, Gan Y, Weimbs T, Simon SM, Rodriguez-Boulan E (2003). Three-dimensional analysis of post-Golgi carrier exocytosis in epithelial cells. Nat Cell Biol 5, 126–136.
Le Bivic A, Sambuy Y, Patzak A, Patil N, Chao M, Rodriguez-Boulan E (1991). An internal deletion in the cytoplasmic tail reverses the apical localization of human NGF receptor in transfected MDCK cells. J Cell Biol 115, 607–618.
Lebreton S, Paladino S, Zurzolo C (2008). Selective roles for cholesterol and actin in compartmentalization of different proteins in the Golgi and plasma membrane of polarized cells. J Biol Chem 283, 29545–29553.
Lisanti MP, Caras IW, Davitz MA, Rodriguez-Boulan E (1989). A glycophospholipid membrane anchor acts as an apical targeting signal in polarized epithelial cells. J Cell Biol 109, 2145–2156.
Lisanti MP, Rodriguez-Boulan E (1990). Glycophospholipid membrane anchoring provides clues to the mechanism of protein sorting in polarized epithelial cells. Trends Biochem Sci 15, 113–118.
Macdonald P, Johnson J, Smith E, Chen Y, Mueller JD (2013). Brightness analysis. Methods Enzymol 518, 71–98.
Malengo G, Andolfo A, Sidenius N, Gratton E, Zamai M, Caiolfa VR (2008). Fluorescence correlation spectroscopy and photon counting histogram on membrane proteins: functional dynamics of the glycosylphosphatidylinositol-anchored urokinase plasminogen activator receptor. J Biomed Opt 13, 031215–031214.
Mattila PE, Kinlough CL, Bruns JR, Weisz OA, Hughey RP (2009). MUC1 traverses apical recycling endosomes along the biosynthetic pathway in polarized MDCK cells. Biol Chem 390, 551–556.
Mattila PE, Youker RT, Mo D, Bruns JR, Cresawn KO, Hughey RP, Ihrke G, Weisz OA (2012). Multiple biosynthetic trafficking routes for apically secreted proteins in MDCK cells. Traffic 13, 433–442.
Mishra R, Grzybek M, Niki T, Hirashima M, Simons K (2010). Galectin-9 trafficking regulates apical-basal polarity in Madin-Darby canine kidney epithelial cells. Proc Natl Acad Sci USA 107, 17633–17638.
Mo D, Costa SA, Ihrke G, Youker RT, Pastor-Soler N, Hughey RP, Weisz OA (2012). Sialylation of N-linked glycans mediates apical delivery of endolyn in MDCK cells via a galectin-9-dependent mechanism. Mol Biol Cell 23, 3636–3646.
Mo D, Potter BA, Bertrand CA, Hildebrand JD, Bruns JR, Weisz OA (2010). Nucleofection disrupts tight junction fence function to alter membrane polarity of renal epithelial cells. Am J Physiol Renal Physiol 299, F1178–F1184.
Naim HY, Joberty G, Alfalah M, Jacob R (1999). Temporal association of the N- and O-linked glycosylation events and their implication in the polarized sorting of intestinal brush border sucrase-isomaltase, aminopeptidase N, and dipeptidyl peptidase IV. J Biol Chem 274, 17961–17967.
Paladino S, Sarnataro D, Pillich R, Tivodar S, Nitsch L, Zurzolo C (2004). Protein oligomerization modulates raft partitioning and apical sorting of GPI-anchored proteins. J Cell Biol 167, 699–709.
Paladino S, Sarnataro D, Tivodar S, Zurzolo C (2007). Oligomerization is a specific requirement for apical sorting of glycosyl-phosphatidylinositol-anchored proteins but not for non-raft-associated apical proteins. Traffic 8, 251–258.
Perroud TD, Huang B, Wallace MI, Zare RN (2003). Photon counting histogram for one-photon excitation. Chem Phys Chem 4, 1121–1123.
Poland PA, Rondanino C, Kinlough CL, Heimburg-Molinaro J, Arthur CM, Stowell SR, Smith DF, Hughey RP (2011). Identification and characterization of endogenous galectins expressed in Madin Darby canine kidney cells. J Biol Chem 286, 6780–6790.
Potter BA, Hughey RP, Weisz OA (2006). Role of N- and O-glycans in polarized biosynthetic sorting. Am J Physiol Cell Physiol 290, C1-C10.
Potter BA, Ihrke G, Bruns JR, Weixel KM, Weisz OA (2004). Specific *N*-glycans direct apical delivery of transmembrane, but not soluble or glycosylphosphatidylinositol-anchored forms of endolyn in Madin-Darby canine kidney cells. Mol Biol Cell 15, 1407–1416.
Qi AD, Wolff SC, Nicholas RA (2005). The apical targeting signal of the P2Y2 receptor is located in its first extracellular loop. J Biol Chem 280, 29169–29175.
Ramadurai S, Holt A, Krasnikov V, van den Bogaart G, Killian JA, Poolman B (2009). Lateral diffusion of membrane proteins. J Am Chem Soc 131, 12650–12656.
Rindler MJ, Ivanov IE, Plesken H, Rodriguez-Boulan E, Sabatini DD (1984). Viral glycoproteins destined for apical or basolateral plasma membrane domains traverse the same Golgi apparatus during their intracellular transport in doubly infected Madin-Darby canine kidney cells. J Cell Biol 98, 1304–1319.
Rodriguez-Boulan E, Gonzalez A (1999). Glycans in post-Golgi apical targeting: sorting signals or structural props. Trends Cell Biol 9, 291–294.
Saffman PG, Delbrück M (1975). Brownian motion in biological membranes. Proc Natl Acad Sci USA 72, 3111–3113.
Salvarezza SB, Deborde S, Schreiner R, Campagne F, Kessels MM, Qualmann B, Caceres A, Kreitzer G, Rodriguez-Boulan E (2009). LIM kinase 1 and cofilin regulate actin filament population required for dynamin-dependent apical carrier fission from the *trans*-Golgi network. Mol Biol Cell 20, 438–451.
Scheiffele P, Roth MG, Simons K (1997). Interaction of influenza virus haemagglutinin with sphingolipid-cholesterol membrane domains via its transmembrane domain. EMBO J 16, 5501–5508.
Schneider D, Greb C, Koch A, Straube T, Elli A, Delacour D, Jacob R (2010). Trafficking of galectin-3 through endosomal organelles of polarized and non-polarized cells. Eur J Cell Biol 89, 788–798.
Sewell R *et al*. (2006). The ST6GalNAc-I sialyltransferase localizes throughout the Golgi and is responsible for the synthesis of the tumor-associated sialyl-Tn *O*-glycan in human breast cancer. J Biol Chem 281, 3586–3594.
Slaughter BD, Huff JM, Wiegraebe W, Schwartz JW, Li R (2008). SAM domain-based protein oligomerization observed by live-cell fluorescence fluctuation spectroscopy. PLoS One 3, e1931.
Slaughter BD, Li R (2010). Toward quantitative "in vivo biochemistry" with fluorescence fluctuation spectroscopy. Mol Biol Cell 21, 4306–4311.
Slaughter BD, Schwartz JW, Li R (2007). Mapping dynamic protein interactions in MAP kinase signaling using live-cell fluorescence fluctuation spectroscopy and imaging. Proc Natl Acad Sci USA 104, 20320–20325.
Stechly L *et al*. (2009). Galectin-4-regulated delivery of glycoproteins to the brush border membrane of enterocyte-like cells. Traffic 10, 438–450.
Stowell SR, Arthur CM, Mehta P, Slanina KA, Blixt O, Leffler H, Smith DF, Cummings RD (2008). Galectin-1, -2, and -3 exhibit differential recognition of sialylated glycans and blood group antigens. J Biol Chem 283, 10109–10123.
Sykes AM, Palstra N, Abankwa D, Hill JM, Skeldal S, Matusica D, Venkatraman P, Hancock JF, Coulson EJ (2012). The effects of transmembrane sequence and dimerization on cleavage of the p75 neurotrophin receptor by γ-secretase. J Biol Chem 287, 43810–43824.
Takeda T, Yamazaki H, Farquhar MG (2003). Identification of an apical sorting determinant in the cytoplasmic tail of megalin. Am J Physiol Cell Physiol 284, C1105–C1113.
Thompson NL (1991). Fluorescence correlation spectroscopy. In: Topics in Fluorescence Correlation Spectroscopy, ed. JR Lakowicz, New York: Plenum, 337–378.
Vilar M *et al*. (2009a). Ligand-independent signaling by disulfide-crosslinked dimers of the p75 neurotrophin receptor. J Cell Sci 122, 3351–3357.
Vilar M *et al*. (2009b). Activation of the p75 neurotrophin receptor through conformational rearrangement of disulphide-linked receptor dimers. Neuron 62, 72–83.
Weisz OA, Rodriguez-Boulan E (2009). Apical trafficking in epithelial cells: signals, clusters and motors. J Cell Sci 122, 4253–4266.
Weisz OA, Swift AM, Machamer CE (1993). Oligomerization of a membrane protein correlates with its retention in the Golgi complex. J Cell Biol 122, 1185–1190.
Wolf-Ringwall AL, Winter PW, Liu J, Van Orden AK, Roess DA, Barisas BG (2011). Restricted lateral diffusion of luteinizing hormone receptors in membrane microdomains. J Biol Chem 286, 29818–29827.
Yeaman C, Le Gall AH, Baldwin AN, Monlauzeur L, Le Bivic A, Rodriguez-Boulan E (1997). The O-glycosylated stalk domain is required for apical sorting of neurotrophin receptors in polarized MDCK cells. J Cell Biol 139, 929–940.
Zurzolo C, van't Hof W, van Meer G, Rodriguez-Boulan E (1994). VIP21/caveolin, glycosphingolipid clusters and the sorting of glycosylphosphatidylinositol-anchored proteins in epithelial cells. EMBO J 13, 42–53.